Continuous Phase Tuning of Vanadium Dioxide Films Using Robust Feedback Mechanism

Jiguo Dai, Chandika Annasiwatta, Ayrton Bernussi, Zhaoyang Fan, Jordan M. Berg and Beibei Ren

***Abstract*—Vanadium dioxide (VO_2) undergoes a metal-insulator transition (MIT) around a temperature close to 68^oC, which enables many digital-like applications including memory devices, sensors, phase change switches, etc. However, the digital-like abruptness of the MIT of VO_2 across a sharp and narrow temperature window limits its usage in the development of applications that demand an analog operation mode with continuously tunable properties. Achieving precise and continuous phase tuning of VO_2 films will enable more powerful and capable devices for analog applications in different fields. Unlike the traditional chemical doping approach which sacrifices the modulation depth, this work incorporates a robust feedback control mechanism into VO_2 films to achieve continuous phase tuning of the intermediate states within the entire phase transition region. In order to attenuate the adverse effect of hysteresis nonlinearity and manufacturing uncertainties associated with the phase transition of VO_2, the uncertainty and disturbance estimator (UDE)-based robust output feedback control approach is developed to achieve the precise continuous phase tuning without using detailed hysteresis modeling information. The effectiveness of the proposed methodology is then verified through an experimental validation.**

I. Introduction

It is well known that the vanadium dioxide (VO_2) undergoes a thermally induced metal-insulator transition (MIT) around a temperature $\sim 68^oC$ [1], [2]. Fig. $1(a)$ and $1(b)$ show that the optical transmittance in the infrared range and the electronic resistance of VO_2 undergo an abrupt change across the MIT region. As seen in Fig. $1(b)$, the electronic resistance of VO_2 could decrease by several orders of magnitude when the temperature increases across the MIT region. Due to this, VO_2 has become a promising functional material in micro-actuation [3], [4], [5], sensors [6], [7], memory devices [8], [9], and optical applications [10], [11], [12], [13], [14].

However, the MIT region of VO_2 exhibits a hysteresis nonlinearity. In other words, the values of physical properties (transmittance, resistance, mechanical stress, etc) lag behind the factors (thermal temperature, voltage, etc) that are controlling them. So, unlike the maximum and minimum

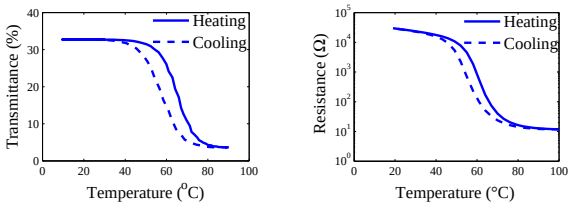

(a) (b)

Figure 1. (a) Transmittance-temperature characteristic of a VO_2 thin film; (b) Resistance-temperature characteristic of a VO_2 thin film.

property values, the intermediate values in the MIT region cannot be attained reliably by tuning the factors. As a result, the use of VO_2 in many applications, like electric switches [15] or optical switches [16], [17], tries to avoid the MIT region and is limited to digital-like ON/OFF states. A thermal signal can be used to trigger the phase transition, leading from a high-resistance/transmittance to a low-resistance/transmittance, i.e., inducing the switching behavior. However, the applicability of VO_2 stands to be broadened if the intermediate states within the phase transition region are better tuned.

The chemical doping is a traditional approach used to continuously tune the MIT property of VO_2 as reported in [16], [18], [19], [20]. By doping VO_2 films with foreign cations like $W^{6+}, Nb^{5+}, Ti^{4+}, Cr^{3+}$ and Al^{3+}, one can modify the shape of MIT region [16]. Specifically, by decreasing the magnitude of the slope of this region, the tuning can be made easier. In [18], by modifying the concentration of tungsten (W) for W-doped VO_2, the gradual tuning of the MIT region and the modulation depth m_T was achieved in a proper range. However, this tuning is achieved by sacrificing the modulation depth [18]. This is not desirable because the performance of many tunable devices is critically dependent on the modulation depth.

Therefore, achieving the precise phase tuning for VO_2 films with a high modulation depth is a challenging problem. This work aims to incorporate the feedback mechanism into the VO_2 films and achieve the precise phase tuning within the full operational range. To tackle with the severe hysteresis nonlinearity as well as the manufacturing uncertainties, both model-based and non-model-based control methodologies have been investigated in the literature. For the model-based control, a hysteresis model is required and an inverse hysteresis model is then implemented to attenuate the hysteresis effect. For example, the Preisach model is studied in [21] to describe the hysteresis phenomenon of optical

Jiguo Dai, Chandika Annasiwatta and Beibei Ren are with the Department of Mechanical Engineering, Texas Tech University, Lubbock, TX 79409, USA, e-mail: jiguo.dai@ttu.edu; chandika.annasiwatta@ttu.edu; beibei.ren@ttu.edu. Their work was supported by the National Science Foundation under Grant CMMI-1728255.

Jordan M. Berg is with the US National Science Foundation, Alexandria, VA, 22314, USA, email: jberg@nsf.gov. His work was supported by the National Science Foundation under the IR/D program.

Ayrton Bernussi and Zhaoyang Fan are with the Department of Electrical and Computer Engineering, Texas Tech University, Lubbock, TX 79409, USA, e-mail: ayrton.bernussi@ttu.edu; zhaoyang.fan@ttu.edu.

and electric properties of a VO_2 sample. In [4], [5], [22], the generalized Prandtl-Ishlinskii (GPI) model is investigated for VO_2-based actuators. However, such hysteresis models are always mathematically complicated and highly sensitive to system parameters. These bring new challenges for the model-based control methodologies. Therefore, a non-model-based controller that is easily implementable and does not rely on much hysteresis model information is preferred. In [23], [24], a classical proportional-integral (PI)-type controller is applied to control a VO_2 integrated micro-actuator, and the deflection can be well controlled. Compared to the PI controller, a novel robust controller called uncertainty and disturbance estimator (UDE)-based robust control [25], [26] has been shown to have a superior robust performance and successfully applied to many practical systems. The main advantage of this robust control methodology is that it can achieve an excellent performance while only using limited system information (i.e., operation bandwidth and steady-state gain). Therefore, this paper adopts the UDE-based robust control for precise phase tuning of VO_2 films, and the optical transmittance is considered as the controlled property.

Once the proposed robust feedback control mechanism can achieve the precise phase tuning of VO_2 within its full operational range, the overall closed-loop system can be regarded as a VO_2 device with a reconfigurable phase transition region. All the intermediate states within the phase transition region can be treated as operational states, and the achieved continuous phase tuning enables the usage of VO_2 device in analog applications.

The rest of this paper is organized as follows. Section II gives the system description and the control problem formulation. The main results are demonstrated in Section III. The experimental validation is provided in Section IV, which is followed by some concluding remarks in Section V. The variables used in this paper are defined as, $y(t)$ is the optical transmittance value of VO_2 films, $y_m(t)$ is the reference signal, $v(t)$ is the temperature of the VO_2 sample, $u(t)$ is the input voltage for the thermoelectric (TE) module, and $u_T(t)$ is a user-defined regulation signal. Furthermore, there are two quantities which are determined by the physical properties of VO_2 films, the modulation depth m_T and the phase transition window width w_T.

II. System Description and Problem Formulation

A. System Description

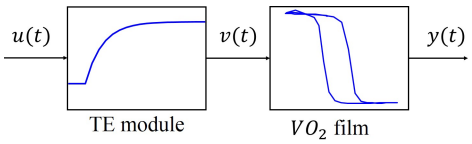

Figure 2. The block diagram for a VO_2 system.

As shown in Fig. 2, the system consists of a VO_2 film and a TE module. By applying a proper control input voltage $u(t)$, the VO_2 film temperature $v(t)$ can be regulated, and the optical transmittance output $y(t)$ will be changed. The temperature-transmittance relationship of the VO_2 film suffers a severe hysteresis nonlinearity. In the literature, the hysteresis nonlinearity can be described by using the Preisach model [21], the GPI model [4], etc. Generally, the following operator (1) can be adopted to represent the hysteresis nonlinearity,

$$y(t) = \Phi[v](t). \tag{1}$$

Furthermore, the dynamics of the TE module can be described as

$$\frac{dv(t)}{dt} = -\alpha_1 \left(v(t) - v_0\right) + \frac{\beta_1 u(t)}{\alpha_2} + \beta_2, \tag{2}$$

where $\alpha_1, \alpha_2, \beta_1$ are physical constants, β_2 is an external disturbance, and v_0 is the ambient temperature. Let $T = \frac{1}{\alpha_1}$, $K = \frac{\beta_1}{\alpha_1 \alpha_2}$, and $\delta(t) = \frac{\beta_2}{\alpha_1} + v_0$, (2) can be expressed as

$$T\dot{v}(t) = -v(t) + Ku(t) + \delta(t). \tag{3}$$

The parameters T and K represent the time constant and the DC gain of the TE module, respectively. $\delta(t)$ represents the total effect of disturbances and uncertainties.

B. Problem Formulation

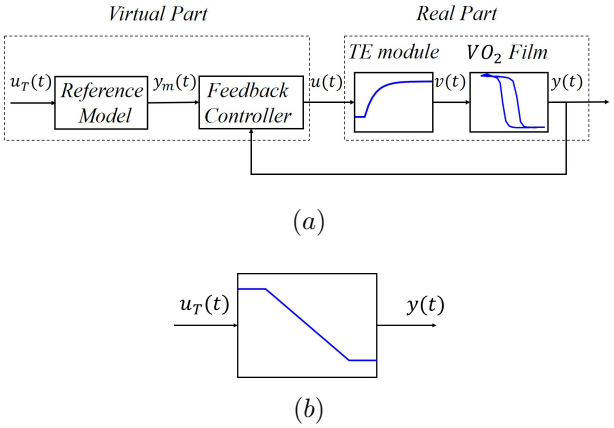

Figure 3. Conception of an empowered VO_2 device with the reconfigurable phase transition.

To empower VO_2 with a reconfigurable phase transition and achieve its full operational range, a feedback structure is proposed as shown in Fig. $3(a)$. In this structure, the real part consists of the VO_2 film and the TE module, while a reference model and a feedback controller form a virtual part. The reference model uses $u_T(t)$ as an input and $y_m(t)$ as its output. A feedback controller can be proposed to regulate the system output $y(t)$ to track the reference signal $y_m(t)$. Consequently, the input-output relationship for the closed-loop system is $u_T(t) \to y(t)$. Unlike the relationship $v(t) \to y(t)$ which exhibits a severe hysteresis nonlinearity with a sharp and narrow temperature window in its phase transition region, the closed-loop relationship $u_T(t) \to y(t)$ is reconfigurable, for example, a linear relationship shown in Fig. $3(b)$. The shape of the reconfigurable phase transition

for the closed-loop system can be determined by a reference model, $h : u_T(t) \to y_m(t)$, which will be designed in Section III-A. Combining (1) and (3), the dynamics of the open-loop system can be described by

$$T\dot{v}(t) = -v(t) + Ku(t) + \delta(t), \quad (4)$$

$$y(t) = \Phi[v](t). \quad (5)$$

This system is a cascaded system with a first-order dynamics (TE module) and a hysteresis nonlinearity (VO_2 sample). The control objective is to find an input voltage $u(t)$ that can regulate the output, i.e., the optical transmittance of VO_2, $y(t)$, to a desired reference signal $y_m(t)$, with the error dynamics satisfying (6),

$$\dot{e}(t) = -ke(t), \quad (6)$$

where $e(t) = y_m(t) - y(t)$ is the tracking error, and $k > 0$ is the error feedback gain which guarantees $\lim_{t\to\infty} e(t) = 0$. Consequently, the relationship $v(t) \to y(t)$ can be reconfigured as the relationship $u_T(t) \to y(t)$.

III. Proposed Feedback Control Mechanism

A. Reference Model

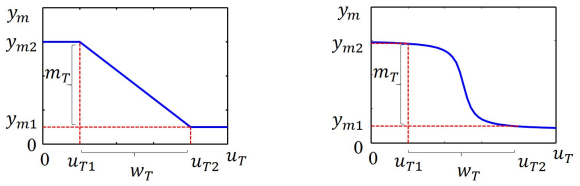

(a) Linear model (8) (b) Nonlinear model (9)

Figure 4. Illustration of reference models.

The reference signal $y_m(t)$ is generated by the following reference model

$$y_m(t) = h(u_T(t), w_T, m_T), \quad (7)$$

where $u_T(t)$ is an analog regulation signal, and w_T and m_T are two constant parameters which represent the regulation window and the modulation depth, respectively. These two parameters are determined by the application demand and the property of the VO_2 sample. h is a monotonic function. The analog regulation signal u_T is limited within $[u_{T1}, u_{T2}]$, where u_{T1}, u_{T2} are lower and upper bounds of the regulation signal u_T. The phase transition window is defined as $w_T = u_{T2} - u_{T1}$. The output $y_m(t)$ is within $[y_{m1}, y_{m2}]$, where y_{m1}, y_{m2} are the minimum and maximum outputs of the VO_2 sample. The modulation depth is defined as $m_T = y_{m2} - y_{m1}$. The reference model can be either linear, e.g.,

$$y_m(t) = h(u_T(t), w_T, m_T) = \begin{cases} -\frac{m_T}{w_T}(u_T(t) - u_{T_1}) + y_{m2}, & u_{T1} \le u_T \le u_{T2} \\ y_{m1}, & u_T < u_{T1} \\ y_{m2}, & u_T > u_{T2} \end{cases} \quad (8)$$

which is illustrated in Fig. 4 (a); or nonlinear, e.g.,

$$y_m(t) = h(u_T(t), w_T, m_T) = \frac{m_T}{2}\tanh(-2(u_T(t) - \frac{w_T}{2} - u_{T1})) + \frac{m_T}{2} + y_{m1} \quad (9)$$

which is illustrated in Fig. 4 (b). The reference models can be designed according to the application demands.

B. Output Feedback Controller based on Uncertainty and Disturbance Estimator (UDE)

In order to avoid the modeling process for hysteresis nonlinearity $\Phi[v]$ in (5), instead of designing control for the original system dynamics (4)-(5) directly, an equivalent transformation, including a first-order linear model plus a lumped uncertainty term, is used to represent the input-output relationship. As shown in [27], one can rearrange the input-output relationship of the system model (4)-(5) by introducing a first-order linear model $\frac{b}{s+a}$ as follows

$$y(t) = \mathcal{L}^{-1}\left\{\frac{b}{s+a}\right\} * u(t) - \mathcal{L}^{-1}\left\{\frac{b}{s+a}\right\} * u(t) + y(t) = \mathcal{L}^{-1}\left\{\frac{b}{s+a}\right\} * u(t) + z(t), \quad (10)$$

where $a > 0$, b has the same sign as the system DC gain, "$*$" is the convolution operator, $\mathcal{L}^{-1}\{\cdot\}$ is the inverse Laplace operator, and

$$z(t) = y(t) - \mathcal{L}^{-1}\left\{\frac{b}{s+a}\right\} * u(t).$$

From (10), there is

$$\dot{y}(t) = -ay(t) + bu(t) + \dot{z}(t) + az(t) = -ay(t) + bu(t) + u_d(t), \quad (11)$$

where

$$u_d(t) = \dot{z}(t) + az(t) \quad (12)$$

is the lumped uncertainty, including the contribution of the (unknown) dynamics, hysteresis, and disturbances of the system. From (11), there is

$$\dot{e}(t) = -ke(t) + [ke(t) + \dot{y}_m(t) + ay(t) - bu(t) - u_d(t)]. \quad (13)$$

In order to achieve (6), the controller can be chosen as

$$u(t) = \frac{1}{b}[\dot{y}_m(t) + ke(t) + ay(t) - u_d(t)]. \quad (14)$$

From (11), there is $u_d(t) = \dot{y}(t) + ay(t) - bu(t)$. Based on the idea of the UDE-based robust control [25], $u_d(t)$ can be estimated with a strictly proper and stable filter $G_f(s)$ as

$$\hat{u}_d(t) = g_f(t) * u_d(t) = g_f(t) * (\dot{y}(t) + ay(t) - bu(t)), \quad (15)$$

where $g_f(t) = \mathcal{L}^{-1}\{G_f(s)\}$ is the impulse response of the filter $G_f(s)$. If this filter has the unity gain and zero phase shift over the spectrum of $u_d(t)$ and zero gain elsewhere, then the estimation is accurate. By replacing $u_d(t)$ in (14)

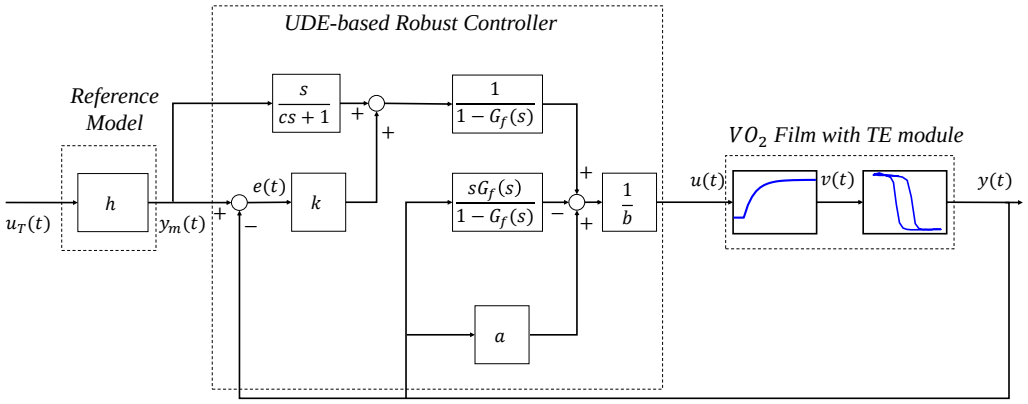

Figure 5. Block diagram for the closed-loop system.

with $\hat{u}_d(t)$ in (15), the UDE-based robust output feedback controller can be obtained as

$$u(t) = \frac{1}{b}\left[ay(t) - \mathcal{L}^{-1}\left\{\frac{sG_f(s)}{1-G_f(s)}\right\} * y(t) + \mathcal{L}^{-1}\left\{\frac{1}{1-G_f(s)}\right\} * (\dot{y}_m(t) + ke(t))\right]. \quad (16)$$

The overall closed-loop system is demonstrated in Fig. 5. In the controller (16), the derivative term $\dot{y}_m(t)$ can be implemented through a low pass filter. More detailed knowledge about the proposed control methodology including the parameter selection and stability analysis can be referred to [27].

C. Performance Analysis

Since the time constant T for the TE module is very large, the lumped uncertainty term $u_d(t)$ is slowly varying. The low-pass filter in the controller (16) can be chosen as

$$G_f(s) = \frac{1}{\tau s + 1}, \quad (17)$$

where $\tau > 0$ is the time constant. The error dynamics for the overall closed-loop system is then obtained as

$$\begin{aligned} \dot{e}(t) &= -ke(t) + \hat{u}_d(t) - u_d(t) \\ &= -ke(t) + \mathcal{L}^{-1}\left\{\frac{-\tau s}{\tau s + 1}\right\} * u_d(t). \end{aligned} \quad (18)$$

Considering the reference signal $y_m(t)$ as a step type, the lumped uncertainty term $u_d(t)$ can be viewed as an unknown step type signal. Consequently, the Laplace transform of $u_d(t)$ can be obtained as $\frac{D}{s}$, where D is an unknown constant. Let e_0 be the initial value of $e(t)$. Therefore, (18) can be written as

$$\dot{e}(t) = -ke(t) - D\exp\left(-\frac{t}{\tau}\right). \quad (19)$$

The tracking error is solved via

$$e(t) = \left(e_0 + \frac{D\tau}{\tau k - 1}\right)\exp(-kt) + \frac{D\tau}{\tau k - 1}\exp\left(-\frac{t}{\tau}\right). \quad (20)$$

In (20), the first part can be made to vanish fast by choosing a large k. The vanishing speed of the second part is determined by τ. It can be seen that the tracking error $e(t)$ could converge to 0 when $t \to \infty$, and the transient performance is determined by k and τ. The larger value of k and the smaller value of τ, the faster the convergence is. However, a very large k may result in control saturation in practice. And there also exists a trade-off for selecting τ as discussed in [26]. A high filter bandwidth (very small τ) will amplify the high frequency measurement noise. Consequently, both k and τ should be selected properly to satisfy the control requirement.

IV. Experimental Validation

The proposed feedback control design is validated through an experiment in this section.

A. Experimental Setup

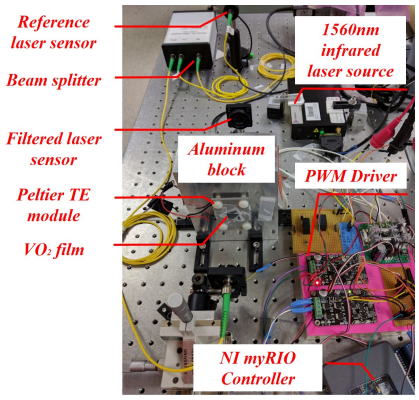

Figure 6. Experimental platform.

Fig. 6 shows the experimental setup for the validation, where a thin W-doped VO_2 sample is attached to an aluminum block (used as a heat sink), and a Peltier TE module is used for heating/cooling the VO_2 sample. A

$1560nm$ infrared laser is directed into a beam splitter and decomposed into 1% and 99% parts. The 1% of input power is used as a reference, and the 99% of the input power is sent through the VO_2 thin film. Thorlabs' PM100USB optical power sensors are used to detect the reference optical power $P_{ref} = 1\%P_{total}$ and the optical power P_{filter} which is being filtered by the VO_2 thin film. Then the optical transmittance is calculated by $y(t) = \frac{P_{filter}}{99P_{ref}} \times 100\%$. The Peltier TE module is driven by the PWM driver and the control signal is generated by a NI myRIO controller. The

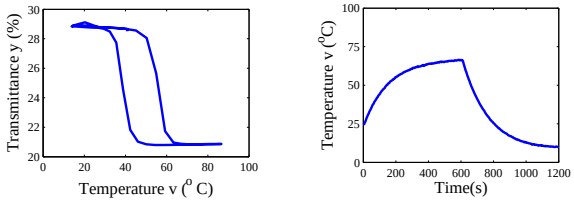

(a) (b)

Figure 7. (a) Hysteresis major loop for a thin W-doped VO_2 sample; (b)Step response of TE module.

sampling time is set as $1.5s$. The hysteresis major loop of the measured temperature-transmittance relationship for the W-doped VO_2 sample is shown in Fig. $7(a)$, where the optical transmittance of the VO_2 sample varies from 21% to 29%. Fig. $7(b)$ shows the step response of the Peltier TE module, where the time constant T of the TE module is identified as $120s$. The performance of the Peltier TE module will be further improved in future work.

B. Experimental Results

To demonstrate the effectiveness of the developed controller (16) for continuous phase tuning within the phase transition region, two cases are considered in this section. The intermediate operational states can be selected within the full operational range of the VO_2 film.

1) Piecewise Continuous Phase Tuning: In this case, the transmittance values of 21%, 25% and 27% are selected as intermediate operational states, and the reference signal $y_m(t)$ is given as

$$y_m(t) = \begin{cases} 25\%, & 0s \sim 500s \\ 21\%, & 500s \sim 1000s \\ 25\%, & 1000s \sim 1500s \\ 27\%, & 1500s \sim 2000s \end{cases}.$$

The reference model can be chosen as

$$y_m(t) = \begin{cases} 21\%, & u_T \in [0, 1) \\ 25\% & u_T \in [1, 2) \\ 27\% & u_T \in [2, 3] \end{cases}.$$

By following the guidelines in [27], the control parameters (16) are chosen as $a = 0.01$, $b = -5$, $G_f(s) = \frac{1}{100s+1}$ and $k = 200$. Fig. 8 shows the piecewise continuous phase tuning results. As shown in Fig. $8(a)$, the optical transmittance of VO_2 film is successfully regulated to the desired

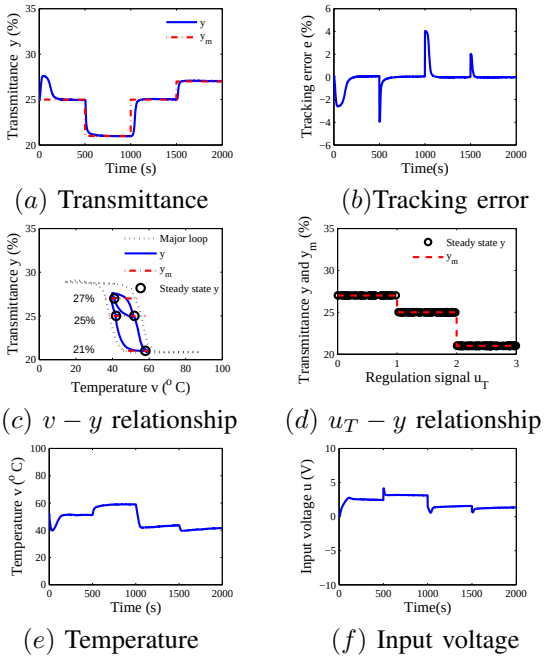

(a) Transmittance (b)Tracking error

(c) $v-y$ relationship (d) u_T-y relationship

(e) Temperature (f) Input voltage

Figure 8. Piecewise continuous phase tuning.

intermediate operational states. The tracking error is plotted in Fig. $8(b)$, where the steady state error is within 0.1%. The temperature-transmittance $(v-y)$ relationship is depicted in Fig. $8(c)$, where the three red dash-dot lines represent three intermediate operational states. It can be seen that the system output y can be successfully regulated to the desired intermediate operational states, 21%, 25% and 27% at steady state. The $u_T - y$ relationship is then demonstrated in Fig. $8(d)$ as piecewise continuous, instead of hysteric. Figs. 8 (e) and (f) illustrate the profiles of the sample temperature and the control input voltage, respectively.

2) Triangular Wave Continuous Phase Tuning: In this case, the intermediate operational states are selected as a continuous triangular wave between 22% and 27% with a period of $1000s$. Then, the reference signal $y_m(t)$ is formulated as

$$y_m(t) = \begin{cases} -0.010t + 27, & 0s \sim 500s \\ 0.010(t - 500) + 22, & 500s \sim 1000s \\ -0.010(t - 1500) + 22, & 1000s \sim 1500s \\ 0.010(t - 1500) + 22, & 1500s \sim 2000s \end{cases}.$$

The reference model can be chosen as

$$y_m(t) = -\frac{5}{3}u_T(t) + 27, \ u_T \in [0, 3].$$

The control parameters are chosen as $a = 0.01$, $b = -5$, $G_f(s) = \frac{1}{30s+1}$ and $k = 300$. The tuning performance is demonstrated in Fig. 9. Fig. $9(a)$ demonstrates the phase tuning performance along the triangular wave reference. The steady state error is also within 0.1%, as shown in Fig. 9 (b). The temperature-transmittance $(v-y)$ relationship in Fig. $9(c)$ illustrates the tuned phase trajectory within the transition region. Fig. $9(d)$ shows the $u_T - y$ relationship as linear.

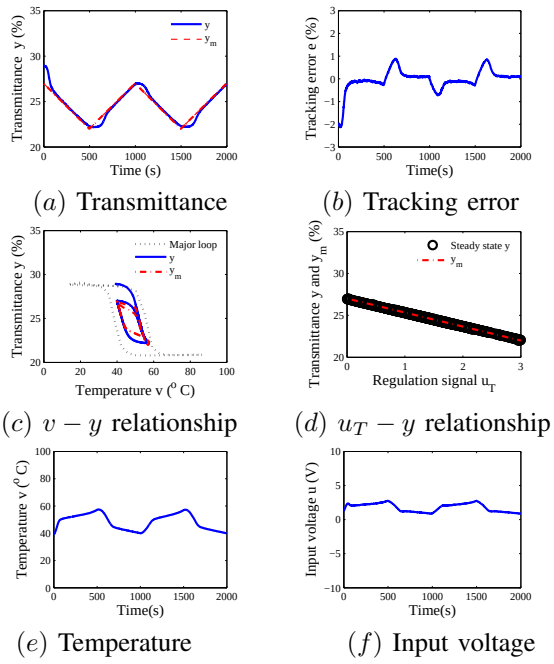

Figure 9. Triangular wave continuous phase tuning.

The profiles of the sample temperature and the control input voltage are shown in Figs. 9 (e) and (f), respectively.

V. Concluding Remarks

In conclusion, the results in the paper have shown the feasibility of applying the feedback control mechanism to achieve continuous phase tuning of VO_2 films within the full phase transition region. With the excellent performance of the UDE-based robust controller, continuous optical transmittance control for VO_2 films has been achieved without using detailed hysteresis modeling information. The phase transition of the composite VO_2 device has been reconfigured by properly selecting a reference model. The effectiveness of the proposed feedback mechanism has been verified via an experimental validation.

References

[1] F. Morin, "Oxides which show a metal-to-insulator transition at the neel temperature," *Physical Review Letters*, vol. 3, no. 1, p. 34, July 1959.

[2] Z. Yang, C. Ko, and S. Ramanathan, "Oxide electronics utilizing ultrafast metal-insulator transitions," *Annual Review of Materials Research*, vol. 41, pp. 337–367, Aug. 2011.

[3] J. Zhang, D. Torres, E. Merced, N. Sepúlveda, and X. Tan, "A hysteresis-compensated self-sensing scheme for vanadium dioxide-coated microactuators," in *Proc. ASME Dynamic Systems and Control Conference*, San Antonio, TX, 2014.

[4] J. Zhang, E. Merced, N. Sepúlveda, and X. Tan, "Modeling and inverse compensation of nonmonotonic hysteresis in VO_2-coated microactuators," *IEEE/ASME Trans. Mechatronics*, vol. 19, no. 2, pp. 579–588, April 2014.

[5] ——, "Modeling and inverse compensation of hysteresis in vanadium dioxide using an extended generalized Prandtl–Ishlinskii model," *Smart Materials and Structures*, vol. 23, no. 12, p. 125017, Oct. 2014.

[6] A. Prasad, S. Amirthapandian, S. Dhara, S. Dash, N. Murali, and A. Tyagi, "Novel single phase vanadium dioxide nanostructured films for methane sensing near room temperature," *Sensors and Actuators B: Chemical*, vol. 191, pp. 252–256, Feb. 2014.

[7] Y. Bu, J. Zou, Y. Liu, Z. Zhu, W. Deng, X. Peng, and B. Tang, "Simple and efficient synthesis of high-quality VO_2 thin films and their application in vacuum sensor with wide pressure range," *Thin Solid Films*, vol. 638, pp. 420–425, Sept. 2017.

[8] H. Coy, R. Cabrera, N. Sepúlveda, and F. E. Fernández, "Optoelectronic and all-optical multiple memory states in vanadium dioxide," *Journal of Applied Physics*, vol. 108, no. 11, p. 113115, Oct. 2010.

[9] Y. Gao, H. Luo, Z. Zhang, L. Kang, Z. Chen, J. Du, M. Kanehira, and C. Cao, "Nanoceramic VO_2 thermochromic smart glass: A review on progress in solution processing," *Nano Energy*, vol. 1, no. 2, pp. 221–246, March 2012.

[10] E. E. Chain, "Optical properties of vanadium dioxide and vanadium pentoxide thin films," *Applied Optics*, vol. 30, no. 19, pp. 2782–2787, July 1991.

[11] P. U. Jepsen, B. M. Fischer, A. Thoman, H. Helm, J. Y. Suh, R. Lopez, and R. F. Haglund, "Metal-insulator phase transition in a VO_2 thin film observed with terahertz spectroscopy," *Physical Review B*, vol. 74, no. 20, p. 205103, Nov. 2006.

[12] J. Singh, *Optical properties of condensed matter and applications*. John Wiley & Sons, 2006, vol. 6.

[13] Z. Huang, S. Chen, C. Lv, Y. Huang, and J. Lai, "Infrared characteristics of VO_2 thin films for smart window and laser protection applications," *Applied Physics Letters*, vol. 101, no. 19, p. 191905, Oct. 2012.

[14] D. Malarde, M. J. Powell, R. Quesada-Cabrera, R. L. Wilson, C. J. Carmalt, G. Sankar, I. P. Parkin, and R. G. Palgrave, "Optimized atmospheric-pressure chemical vapor deposition thermochromic VO_2 thin films for intelligent window applications," *ACS Omega*, vol. 2, no. 3, pp. 1040–1046, March 2017.

[15] G. Stefanovich, A. Pergament, and D. Stefanovich, "Electrical switching and mott transition in VO_2," *Journal of Physics: Condensed Matter*, vol. 12, no. 41, p. 8837, 2000.

[16] F. Beteille and J. Livage, "Optical switching in VO_2 thin films," *Journal of Sol-Gel Science and Technology*, vol. 13, no. 1-3, pp. 915–921, Jan. 1998.

[17] S. Bonora, U. Bortolozzo, S. Residori, R. Balu, and P. Ashrit, "Mid-IR to near-IR image conversion by thermally induced optical switching in vanadium dioxide," *Optics Letters*, vol. 35, no. 2, pp. 103–105, Jan. 2010.

[18] G. Karaoglan-Bebek, M. N. F. Hoque, M. Holtz, Z. Fan, , and A. A. Bernussi, "Continuous tuning of W-doped VO_2 optical properties for terahertz analog applications," *Applied Physics Letters*, vol. 105, p. 201902, Nov. 2014.

[19] M. N. F. Hoque, G. Karaoglan-Bebek, M. Holtz, A. A. Bernussi, and Z. Fan, "High performance spatial light modulators for terahertz applications," *Optics Communications*, vol. 350, pp. 309–314, Sept. 2015.

[20] J. Jian, X. Wang, L. Li, M. Fan, W. Zhang, J. Huang, Z. Qi, and H. Wang, "Continuous tuning of phase transition temperature in VO_2 thin films on c-cut sapphire substrates via strain variation," *ACS Applied Materials & Interfaces*, vol. 9, no. 6, pp. 5319–5327, Jan. 2017.

[21] A. W. C. D. Annasiwatta, J. Chen, J. M. Berg, A. Bernussi, Z. Fan, and B. Ren, "Modeling hysteresis in vanadium dioxide thin films," in *Proc. American Control Conference*, Sept. 2016, pp. 6905–6910.

[22] M. A. Janaideh, S. Rakheja, and C.-Y. Su, "An analytical generalized Prandtl-Ishlinskii model inversion for hysteresis compensation in micropositioning control," *IEEE/ASME Trans. Mechatronics*, vol. 16, no. 4, pp. 734–744, July 2011.

[23] J. Zhang, D. Torres, J. L. Ebel, N. Sepúlveda, and X. Tan, "A composite hysteresis model in self-sensing feedback control of fully integrated VO_2 microactuators," *IEEE/ASME Transactions on Mechatronics*, vol. 21, no. 5, pp. 2405–2417, Oct. 2016.

[24] E. Merced, X. Tan, and N. Sepúlveda, "Closed-loop tracking of large displacements in electro-thermally actuated VO_2-based mems," *Journal of Microelectromechanical Systems*, vol. 23, no. 5, pp. 1073–1083, Feb. 2014.

[25] Q.-C. Zhong and D. Rees, "Control of uncertain LTI systems based on an uncertainty and disturbance estimator," *ASME Trans. J. Dyn. Sys. Meas. Control*, vol. 126, no. 4, pp. 905–910, Dec. 2004.

[26] B. Ren, Q.-C. Zhong, and J. Dai, "Asymptotic reference tracking and disturbance rejection of UDE-based robust control," *IEEE Trans. Ind. Electron.*, vol. 64, no. 4, pp. 3166–3176, Apr. 2017.

[27] J. Dai, B. Ren, and Q.-C. Zhong, "Output feedback trajectory tracking control via uncertainty and disturbance estimator," in *Proc. American Control Conference*, Milwaukee, WI, USA, June 2018, pp. 2139–2144.